Vaporizing Liquid Microthrusters with integrated heaters and temperature measurement

Silva, Marsil A.C.; Cordeiro Guerrieri, D.; van Zeijl, Henk; Cervone, Angelo; Gill, Eberhard

DOI
10.1016/j.sna.2017.07.032

Publication date
2017

Document Version
Accepted author manuscript

Published in
Sensors and Actuators A: Physical: an international journal devoted to research and development of physical and chemical transducers

Citation (APA)
Silva, M. A. C., Cordeiro Guerrieri, D., van Zeijl, H., Cervone, A., & Gill, E. (2017). Vaporizing Liquid Microthrusters with integrated heaters and temperature measurement. *Sensors and Actuators A: Physical: an international journal devoted to research and development of physical and chemical transducers*, *265*, 261-274. https://doi.org/10.1016/j.sna.2017.07.032

Vaporizing Liquid Microthrusters with integrated heaters and temperature measurement

Marsil A. C. Silva[a,*], Daduí C. Guerrieri[a], Henk van Zeijl[b], Angelo Cervone[a], Eberhard Gill[a]

[a] *Faculty of Aerospace Engineering, TU Delft, The Netherlands*
[b] *Else Kooi Laboratory, TU Delft, The Netherlands*

Abstract

This paper presents the results of design, manufacturing and characterization of Vaporizing Liquid Microthrusters (VLM) with integrated heaters and temperature sensing. The thrusters use water as the propellant and are designed for use in CubeSats and PocketQubes. The devices are manufactured using silicon based MEMS (Micro Electro Mechanical Systems) technology and include resistive heaters to vaporize the propellant. The measurements of the heaters' resistances are used to estimate the temperature in the vaporizing chamber. The manufacturing process is described as well as the characterization of the thrusters' structural and electrical elements. In total 12 devices with different combinations of heaters and nozzles have been assessed and four of them have been used to demonstrate the successful operation of the thrusters. Results show a performance close to the design parameters and are used to validate the thrusters.

Keywords: microresistojet, microthruster, MEMS

1. Introduction

Nano- and pico-satellites have grown in popularity in the last decades as these spacecraft have been applied in a wide range from industrial to educational

*Corresponding author
Email address: m.deathaydecostaesilva@tudelft.nl (Marsil A. C. Silva)

applications. They have also been used to demonstrate novel technologies and as tools especially for Earth observation [1, 2, 3]. The maturity of this class of satellites is high but the research on micropropulsion for these spacecraft is still at an early stage and the systems are not yet at the required maturity.

Micropropulsion systems can be applied for a variety of functions, such as the execution of precise orbital and attitude maneuvers which are important for the execution of missions such as space debris removal, orbit transfer, and formation flying. Recently, many different micropropulsion systems have been developed particularly focused on the implementation on CubeSats [4].

Within micropropulsion systems, microresistojets are a very interesting choice, specifically for CubeSats, since it is one of the few types of such systems currently able to achieve a thrust level in the range 1–10 mN while still meeting all the constraints posed by extremely miniaturized spacecraft. The principle of microresistojets is based on heating a gaseous propellant with a resistance and then accelerating and expelling it to space. Some devices use propellants stored in liquid or solid phase, hence a phase-change process is required prior to the heating of the gas. The phase-change is done by heating a resistance in contact with the propellant that is kept in certain conditions of pressure and temperature to allow the phase change (sublimation or vaporization) to occur. Devices that use liquid propellants are called Vaporizing Liquid Microthrusters (VLM) and has been investigated by different research groups as will be discussed in the sequel.

Different designs can be found in the literature reporting the development of microresistojets. In [5] a micro-thruster is presented and tested; it consists of layers of ceramic. The micro-thruster is built by combining three layers of ceramic material: the combustion chamber, the inlet channel, and the nozzle are cut in the inner layer and a micro-heater is attached to the third layer. Tests were performed using water as propellant and it was found that the ceramic thruster is slightly more efficient than some silicon thrusters with respect to power consumption and delivered thrust. Authors in [6] present the details of fabrication and test of a low temperature co-fired ceramic (LTCC) micro-

thruster. They analyze the results for pressure, temperature, power and thrust and also present some comments about the relation between the temperature of the chamber and the vaporization of the propellant.

In [7] the design, simulation, fabrication and test of a VLM are presented. The design of the chamber is based on basic calculations with temperature and residence time. The inlet channel is designed to reduce the pressure drop caused by the friction (which is high for diameters below 500 µm).

Authors in [8] describe the fabrication and test of a vaporizing liquid micro-thruster whose nozzle points in the direction normal to the chip plane. They built and tested two devices with different nozzle exit areas and tested them under different power conditions to characterize the thrust level per applied power.

The analytical modeling of a vaporizing liquid micro-thruster is shown in [9]. The thruster is the same presented in [8]. They focus on the formulation of the equations to calculate the power necessary to vaporize the liquid.

In [10] four micro resistojets were fabricated using MEMS technology and silicon wafers. The main differences among them are the type of nozzle (convergent or divergent) and the chamber volume (300 µm × 750 µm and 600 µm × 1500 µm).

Authors in [11] present the design and manufacturing techniques used to construct a micro resistojet consisting of an inlet portion, a heating section with one or more long channels, and a nozzle. Some tests were performed with three different devices: two with only one channel between the inlet and the nozzle with 10 µm and 5 µm wide, and other with 3 channels and 10 µm wide nozzle.

The devices found in literature often make use of complicated experimental setups including high performance data acquisition systems that might be incompatible with the limitations imposed by very small satellites such as CubeSats specially due to budgetary constrains since usually these satellites make extensive use of commercial-off-the-shelf components. Also, interfacing such a system to external components is always a challenge since these complex devices

integrate fluidic, electrical, and mechanical characteristics into a very small device that also needs a reliable way of sensing the important parameters such as pressure and temperature.

In this paper, we present the design of VLMs with integrated heating and sensing capabilities that allow the easy operation of the microthrusters using standard commercial-off-the-shelf equipment. The devices are designed to meet the strict requirements of nano- and pico-satellites such as CubeSats and PocketQubes and operate using water as the propellant [12]. It has been shown that water is an interesting choice for micropropulsion applications as it can provide a very high Δv per volume when compared to other green propellants [13] making it very interesting for applications where orbital maneuvers are required. The heaters are made out of molybdenum which is a metal that can withstand very high temperatures (melting point 2693 °C) and can be patterned with standard dry or wet etching methods [14]. The resistivity of molybdenum is linearly proportional to the temperatures up to 700 °C allowing the design of heaters that also need precise temperature measurements as in the case of the VLMs. The structural design of the thrusters is based on previous work done in [15]. A special interface combining fluidic, electric, and mechanic connections has been developed to facilitate the operations of the thrusters right after dicing. The results of manufacturing and characterization of the VLMs are presented demonstrating the operations including feedback use of measurements of pressure and temperature. The devices have been manufactured with silicon wafers and tested under near-operational conditions in terms of pressure, mass flow, and power.

The remainder of this paper is organized as follows: section 2 presents the background theory, 3 describes the designs of the thrusters, 5 shows the details of the experiments, the manufacturing process is described in 4, 6 presents the results of the tests, and finally 7 concludes the paper.

2. Background

2.1. Propulsion

The performance of micropropulsion systems can generally be analyzed using the same formulation as in normal sized systems. However, it is important to note that this formulation uses a set of assumptions that might not be applicable to micropropulsion systems as, for example, the assumption of negligible friction forces [16]. Thus, the following set of equations are used only to give insights into the ideal performance of such micropropulsion systems. In this case, two parameters are of major interest when analyzing the performance of the thruster: specific impulse and thrust [16]. The thrust (F in equation 1) is the force generated by the gas accelerated and expelled through the nozzle.

$$F = \dot{m}V_e + (p_e - p_a)A_e \tag{1}$$

where $\dot{m}$ is the mass flow rate, V_e is the exhaust velocity, p_e and p_a the exit and ambient pressures, and A_e is the exit area. The exhaust velocity can be calculated by 2 where M_e is the Mach number at the exit, k is the ratio of the specific heat at constant pressure and constant volume, T_1 is the chamber temperature, and R is the specific gas constant.

$$V_e = M_e\sqrt{kRT_1} \tag{2}$$

The mass flow rate can be written as a function of the chamber (stagnation) pressure and temperature (p_1 and T_1) and the area of the throat A_t:

$$\dot{m} = A_t p_1 k \frac{\sqrt{\left(\frac{2}{k+1}\right)^{\frac{k+1}{k-1}}}}{\sqrt{kRT_1}} \tag{3}$$

Equations 4 to 6 are used to calculate the Mach number, temperature, and pressure at the exit.

$$\frac{A_e}{A_t} = \left(\frac{k+1}{2}\right)^{-\frac{k+1}{2(k-1)}} M_e^{-1}\left(1 + \frac{k-1}{2}M_e^2\right)^{\frac{k+1}{2(k-1)}} \tag{4}$$

$$T_e = T_1 \left(1 + \frac{(k-1)}{2} {M_e}^2 \right)^{-1} \tag{5}$$

$$p_e = p_1 \left(1 + \frac{(k-1)}{2} {M_e}^2 \right)^{\frac{-k}{k-1}} \tag{6}$$

The specific impulse I_{sp} is a measure of efficiency regarding the consumption of propellant.

$$I_{sp} = \frac{F}{\dot{m} g} \tag{7}$$

where $g = 9.806\,65\,\mathrm{m\,s^{-2}}$ is the gravitational acceleration on Earth at sea level. Although the unit is given in seconds, it does not represent a measure of time but a measure of thrust per unit weight of propellant and it should be as high as possible for best propellant consumption efficiency.

Equations 1-7 are used to estimate the performance of the thrusters given the conditions of the experiments and the mechanical characterization of the devices.

2.2. Temperature dependent resistivity

The resistance of the heaters depends on the temperature and might be approximated by the following linear relation:

$$\alpha = \frac{R - R_0}{R_0 \left(T - T_0 \right)} \tag{8}$$

where R is the resistance, T is the current temperature, and R_0 is the resistance measured at temperature T_0. The value of α can be characterized for each device and later used to estimate the temperature of the heaters. As the devices are very small and made of silicon which is good thermal conductor, a zero gradient of temperature might be assumed for the device. Therefore we can estimate that the temperature of the whole device is the same as the one estimated for the heaters. This approach has also been used to characterize similar devices made of Molybdenum [14].

3. Design description

The microresistojets are composed of three main parts: a nozzle, a vaporizing chamber, and a heater. Each of these parts have different designs [17]. There are three types of nozzle named long nozzle, wide nozzle, and bell nozzle indicated in figure 1 as Nozzle 1, Nozzle 2 and Nozzle 3. The geometry and the area ratio (i.e. the ratio between the exit area of the nozzle and the throat area) are what differentiates them; the long nozzle has an area ratio of approximately 11, the wide nozzle 17, and the bell nozzle 11. For the vaporizing chamber there are four designs: diamond pillars that can be large or small with a total surface area of $7.09 \times 10^{-6}\,\mathrm{m}^2$ and $2.27 \times 10^{-5}\,\mathrm{m}^2$ shown in figure 1 as Channel 2 and Channel 4 respectively, and serpentine channels that can be large or small with a total surface area of $5.40 \times 10^{-6}\,\mathrm{m}^2$ and $5.16 \times 10^{-6}\,\mathrm{m}^2$ shown in 1 as Channel 1 and Channel 3 respectively. Finally, there are two types of heaters. One heater type containing 21 lines divided into three sets of 7 lines and the other containing 30 lines divided into sets of 2 lines; in both configurations the lines are 12 µm wide and 3000 µm long. Considering a sheet resistance of around $2\,\Omega\,\square^{-1}$ [14] the total resistance of each heater should be $3.40\,\Omega$ and $2.38\,\Omega$ respectively according to the following equation:

$$R = R_{sh}\frac{L}{W} \tag{9}$$

where R is the resistance, R_{sh} is the sheet resistance, L is the length of the resistance, and W is the width of the resistance.

The mask used during manufacturing containing all the needed features is presented in figure 1. The channels and the heaters are made in a modular manner such that a successive exposure of the slots is needed to make the complete chamber. Each module is designed to produce 1 W of power given a voltage of 5 V. In this case, seven modules are used in order to produce 7 W of power with 5 V which is the middle between maximum and minimum power needed for the thrusters as we will see in the next sub-section. The details of the channels are shown in figure 2. The dimensions are expected to be slightly

different in the manufactured devices due to isotropic etching of the walls that erode approximately by 20 µm.

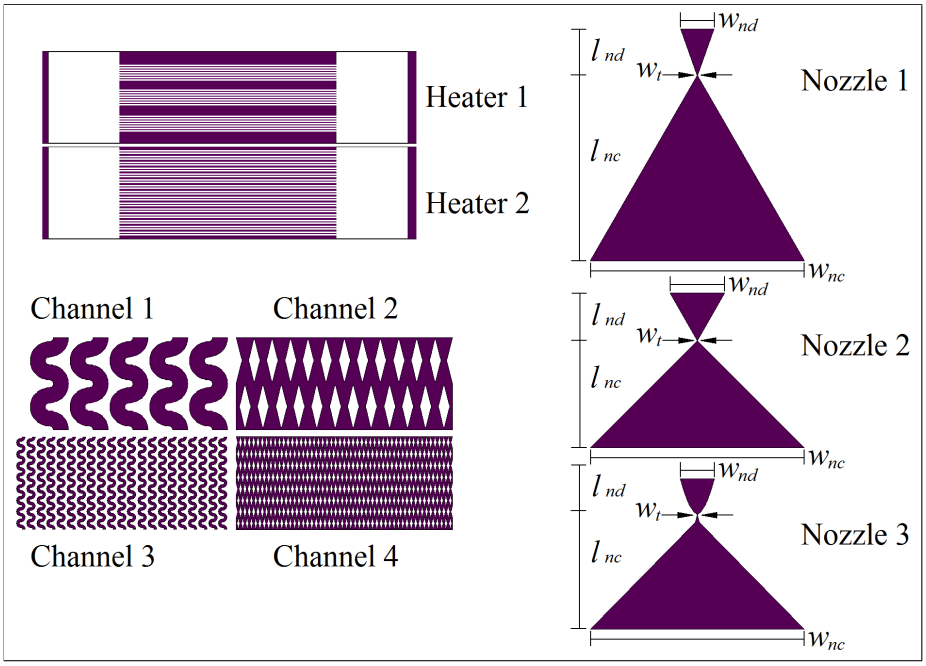

Figure 1: Masks used in the manufacturing of the thrusters. The indexes *nc* and *nd* stand for the convergent and divergent parts of the nozzle respectively and the index *t* stands for the throat part of the nozzle. Dimensions are shown in table 3.

3.1. Performance parameters

With the design parameters of the nozzles, one can estimate the values of thrust and specific impulse given the conditions in the chamber using the equations introduced in sub-section 2.1. Assuming that the system is in the saturation point due to the boiling, the temperature in the chamber will vary in the range from 100 to 150 °C with the pressure in the range from 1 to 5 bar. Note, however, that it is still possible to heat the vapor to a higher temperature by providing more power to the heaters. With these conditions the thrust and specific impulse are calculated using the equations presented in section 2 using the saturation temperature and pressure. The thrust and specific impulse for

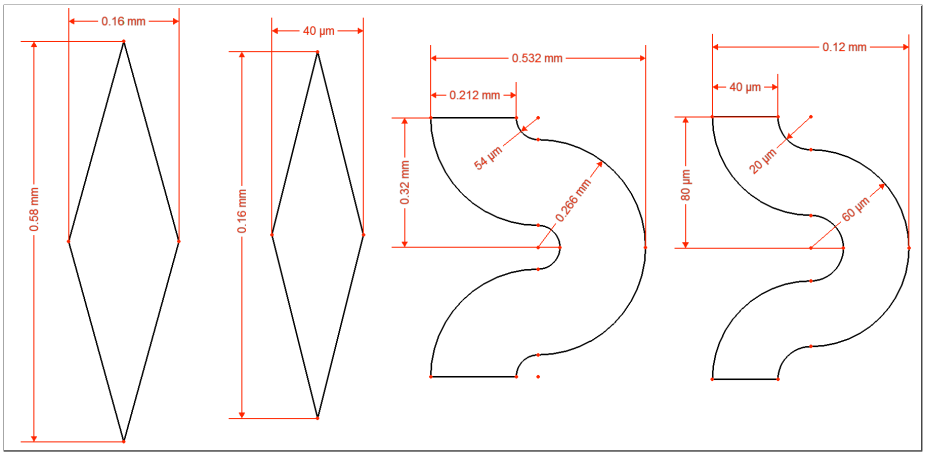

Figure 2: Details of the design parameters of the channels. From left to right: large diamonds, small diamonds, large serpentine, and small serpentine.

the long nozzle and the bell nozzle are the same as they have the same area ratio, respectively $F = 0.75$–$3.79\,\mathrm{mN}$ and $I_{sp} = 105$–$113\,\mathrm{s}$. The wide nozzle is expected to have a slightly higher thrust $F = 0.77$–$3.86\,\mathrm{mN}$ and specific impulse $I_{sp} = 107$–$115\,\mathrm{s}$. As all nozzles have the same throat area, the mass flow rate is the same for all of them in the range $\dot{m} = 0.73$–$3.42\,\mathrm{mg\,s^{-1}}$. The power P necessary to heat-up the water from room temperature of $26.85\,^{\circ}\mathrm{C}$ to boiling point and vaporize it is calculated according to the following equation:

$$P = \Delta E \dot{m} \tag{10}$$

where $\Delta E = E_V - E_L$, E_V is the enthalpy of water vapor at boiling temperature, and E_L is the enthalpy of liquid water at room temperature. For the given mass flow rates, the power lies in the range $P = 1.87$–$9.01\,\mathrm{W}$.

4. Manufacturing

The starting material is a 100 mm double side polished silicon wafer with thickness of 300 µm. A layer of 500 nm of LPCVD (low pressure chemical vapor deposition) silicon nitride is deposited on the wafer to isolate the substrate from

the heaters. Then, a layer of 200 nm of molybdenum is deposited on the front side of the wafer by sputtering. To form a hard mask for patterning Mo, a layer of PECVD TEOS (Plasma-enhanced chemical vapor deposition tetraethoxysilane) is deposited. The mask for the heaters is made with photoresist and the patterning is done first for TEOS (hard mask) by wet etching with buffered hydrofluoric acid (BHF) for approximately 2 min. Mo is etched with aluminum etch at 35 °C for approximately 26 s. A schematic cross-section of the device is shown in figure 4.

After stripping off the photoresist with plasma cleaning and removing TEOS with BHF, a layer of 5 µm of silicon dioxide is deposited on both sides to form the hard mask of the cavities (chamber and inlet hole). Photoresist is used to form the soft mask for SiO_2 which is etched with plasma etching. The layer of silicon nitride is also etched in this step with a different recipe. The cavities of the chamber are etched in silicon using a combination of isotropic and anisotropic deep reactive ion etching (DRIE). The isotropic step is done in order to make sure that the narrow channels are successfully opened. The fluid inlets are isotropically etched with DRIE from the heater side after the deposition of a layer of silicon dioxide on the chamber side.

Following the cleaning and removal of the hard masks, the silicon wafer is bonded to a glass wafer with anodic bonding at 400 °C and 1000 V. The glass is intended to provide a good visualization of the flow inside the thruster. This helps to understand the dynamics of the two-phase flow inside the chamber. The last step of manufacturing is dicing. Then the thrusters are ready for tests. A sample diced wafer and a thruster are shown in figure 3. The flow is from the bottom to the top: the propellant enters by the inlet hole, passes by the chamber where it is vaporized and is expelled to the environment by the nozzle. The area after the nozzle is added in order to have a safe path for the cutting blade during dicing; as show in section 3 the nozzles can have different lengths. Therefore this area is to make sure that the shorter nozzles are open.

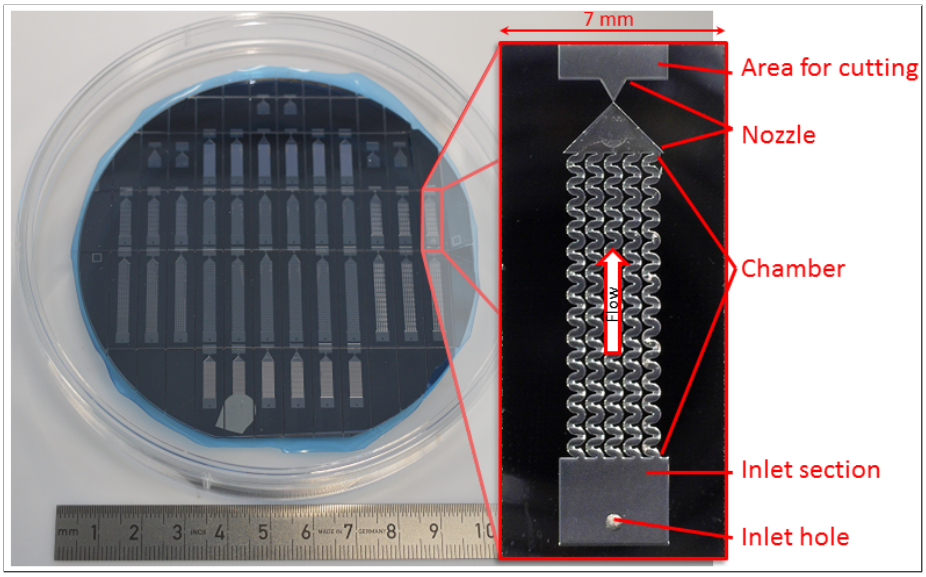

Figure 3: In total each processed wafer yields 36 different devices plus 6 nozzle-only thrusters. In the right, one of the thrusters installed in the interface.

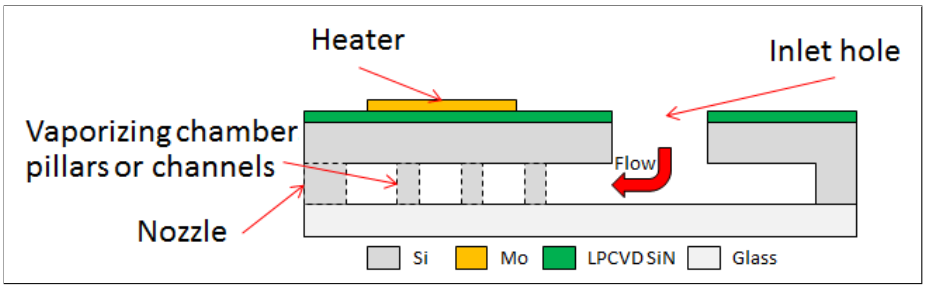

Figure 4: Schematic cross-section of the thrusters. The chamber can be either with diamond pillars or serpentine channels.

5. Experiment Description

Two wafers have been processed using the steps described above. The first one was made without the inlet holes while the second was completely processed. The first wafer is intended to be used for electrical and mechanical tests only and was also used to first assess the bonding process. For these applications, the inlet hole is not needed. A single wafer yields 42 different devices that combine

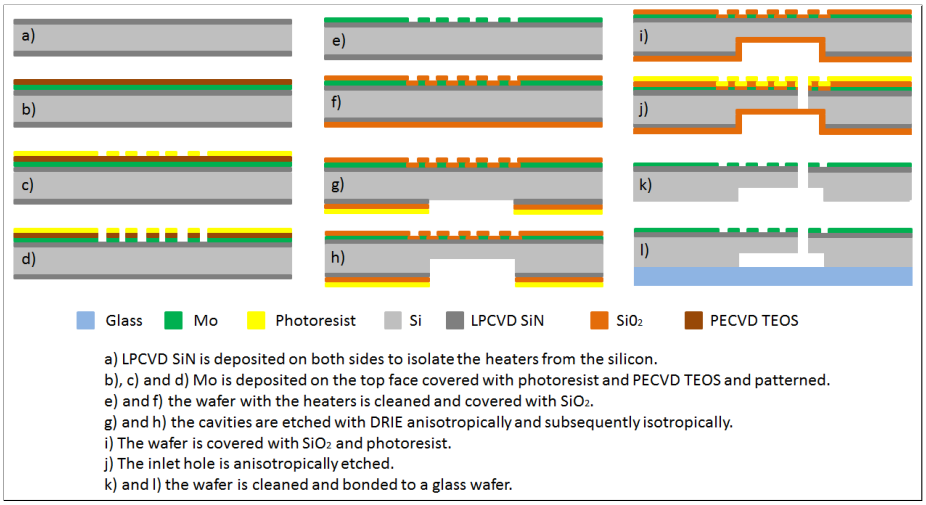

Figure 5: Process flow diagram showing the steps of the manufacturing.

the different options described in section 3. We selected ten thrusters for the mechanical and electrical experiments and four of them went through a further step of characterization to validate the devices in near-operational conditions. The complete list of thrusters is given in table 2. Two devices (number 6 and 8) were found blocked, i.e. no flow can go from the inlet to the nozzle. This is probably due to incomplete etching or a defect caused by particles present during the manufacturing. The thrusters received an identifier that describes the different design options. The code is in the form 'XX-ABx-nn' where 'XX' is the wafer number (00 or 01), 'A' is the type of nozzle (L - long, W - Wide, B - bell), 'B' is the type of chamber (d - diamond small, 'D' - diamond large, 's' - serpentine small, 'S' - serpentine large), 'x' is the type of heater (1 - 21 lines, 2 - 30 lines), and 'nn' is the thruster number in case of repetition.

Table 1: Codes used to identify the different thrusters.

Nozzle	L - Long	W - Wide	B - Bell	
Chamber	d-Diamond small	D-Diamond large	s-Serpentine small	S-Serpentine large
Heater	1 - 21 lines	2 - 30 lines		

The test setup for the measurements is depicted in figure 6. It comprises a computer that controls the power supply for the heaters and the syringe pump used to pump water inside the thrusters at the desired flow rates. The data of temperature and pressure from the interface of the thruster is sent to the computer which also measures the voltage and current levels of the power supply. For the electrical characterization of the resistances, no water is injected into the thruster.

Table 2: List of selected thrusters. Test 1 is the mechanical test, test 2 is the electrical test, and test 3 is the operational test. The codes are presented according to the description given in table 1

Thruster	Code	Test 1	Test 2	Test 3	Detail
1	00-LD1-01	×	×		no inlet
2	00-Ld1-01	×	×		no inlet
3	00-WD2-01	×	×		no inlet
4	00-Bd2-01	×	×		no inlet
5	01-LS1-01	×	×	×	
6	01-BD1-01	×	×		nozzle blocked
7	01-BS2-01	×	×	×	
8	01-WS2-01	×	×		nozzle blocked
9	01-Ld1-01	×	×	×	
10	01-WD2-01	×	×	×	
11	01-Ws1-01	×			
12	01-Bs2-01	×			

A special interface, shown in figure 7, has been designed made out of Teflon and aluminum to allow the easy operation of the thrusters. This interface provides the means for electrical connection to the heaters and also a leak-free connection for the propellant feeding line. Also, a digital sensor measures the pressure and temperature of the liquid being injected into the thruster. The sensor is a MS5837-30BA [18] and measures pressures in the range 0–30 $\pm$ 0.1 bar and temperatures in the range from -20–$85 \pm 4\,^{\circ}\mathrm{C}$.

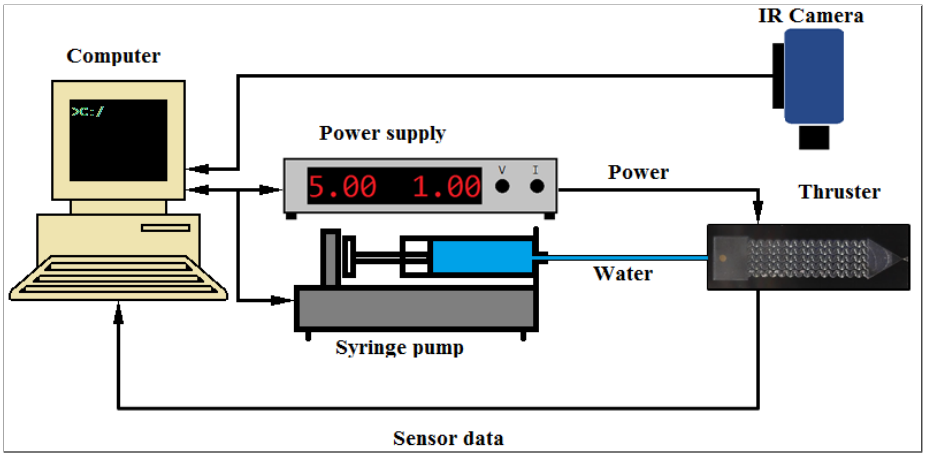

Figure 6: Test configuration for electrical and operational characterization. The infra-red camera is only used during the electrical characterization.

5.1. Mechanical characterization

All the devices have been subject to a mechanical characterization in order to evaluate the dimensions of the features and compare them with the designed values. Table 3 presents the design parameters for the structures. The values d_1 and d_2 refer to the dimensions of the channels. In the case of diamond pillars, these are the sizes of the diamonds as indicated in figure 2; in the case of serpentine channels, these are the inner and outer radii of the semi-circles. The surface roughness is also characterized in order to evaluate the results of the last step of the etching process (isotropic etching). The effect of the surface roughness is an important parameter that affects the performance of microthrusters and has been reported elsewhere [19, 20].

5.2. Electrical characterization

The devices were subject to a resistance test in order to characterize the temperature resistance coefficient α. The test consists in applying a constant voltage to the heaters, measuring the current passing through them, and recording images with the thermal camera. Figure 8 shows a sequence of images taken with the infra-red camera from the nozzle exit plane. The nozzle face of the

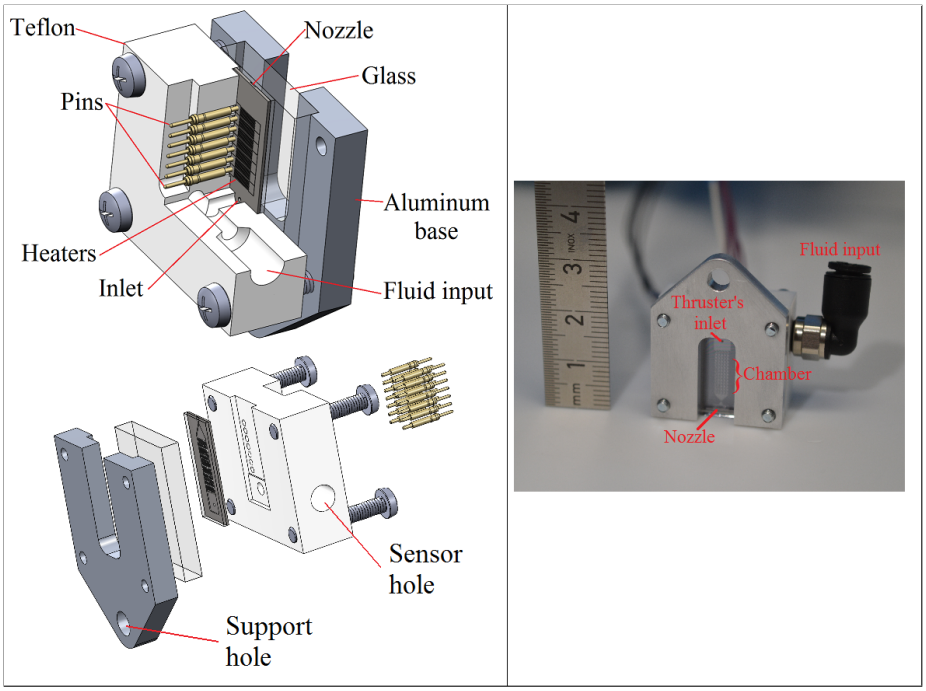

Figure 7: Interface for easy operation of the thrusters. Top left corner: a cut showing the details of the pins and the fluidic channels; bottom left corner: an exploded view of the 3D model; right side: a photo of the interface. The pressure and temperature sensor are on the side opposite to the fluid input. The spring loaded pins connect the heaters to the power supply.

thruster is in the middle of the image where we see the highest temperatures. Thus, the flow vector is normal the plane of the picture. This approach provides an acceptable estimation of the temperature, given the assumption that the whole thruster is at the same temperature.

The images of the thermal camera are then used to estimate the average temperature of the thruster over time. This average temperature is used to estimate α for each thruster. The test starts with applying very low power to the heaters in order to measure the initial resistance. Then the power is increased in two steps applying first 5 V till the temperature stabilizes at a certain value (i.e. reaches steady state) and 7 V till it reaches steady state. In total, 10 devices have been calibrated with this method.

Table 3: Parameters used in the design of the thrusters. All dimensions are in µm. Type descriptions can be found in table 1.

Type	w_{nd}	l_{nd}	w_{nc}	l_{nc}	w_t	d_1	d_2
L	500	645	3000	2600	45		
W	780	660	3000	1500	45		
B	500	500	3000	1600	45		
d						160	40
D						580	160
s						60	20
S						266	54

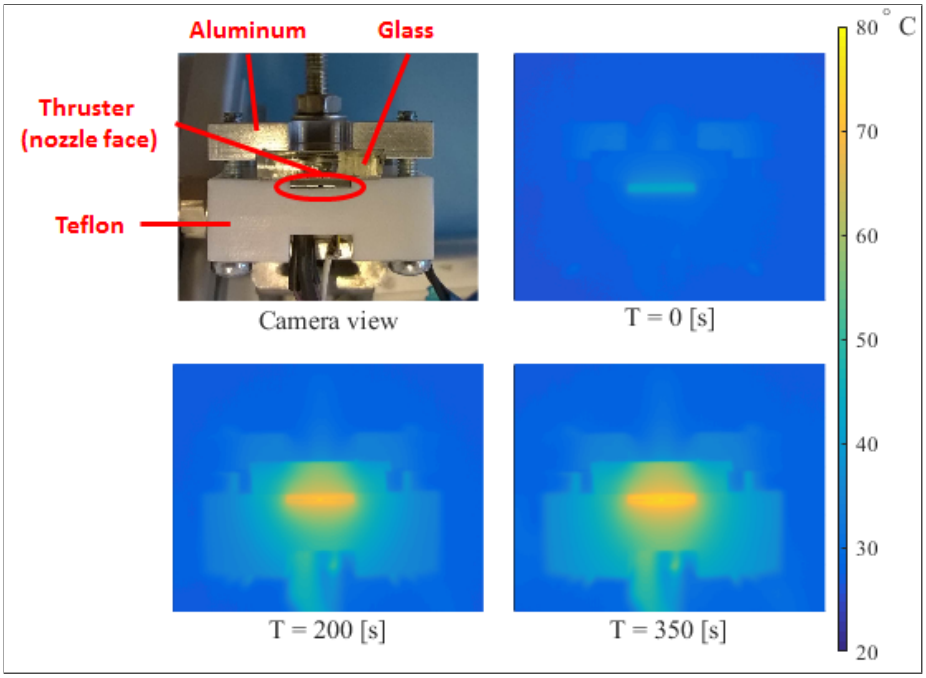

Figure 8: Thermal images of different moments of the test.

Based on the measurements for each device, the value of α is estimated using (8).

5.3. Operational characterization

In the last step of characterization, four devices have been tested in order to validate the devices in near-operational conditions. The test consists of injecting water into the thruster and applying power to the heaters to vaporize the water. The data from the sensors, i.e. pressure and temperature, and from the power supply is collected and also used during the tests as feedback information for manual control of the input variables (flow rate and power).

Water is pumped into the thrusters using a NE-1000 pump with a glass syringe of 2.5 mL to provide a constant mass flow rate sufficient to achieve a pressure of 5 bar in the vaporizing chamber. Although it is a reliable way of controlling the thrusters, it is only applicable for experimental testing since in does not represent the system as in the real application which will consist of a pressurized tank that provides the propellants to the thruster. Also, the syringe pump causes low frequency pressure fluctuations in the flow [21, 22, 23]. These fluctuations might affect the stability of the two-phase flow inside the chamber (i.e. droplets can be ejected during the peaks in pressure).

The manual control is done based on the visual behavior of the vaporization. The power and mass flow rate are manually set to such values that correspond to a complete vaporization of the water without spotting any droplets coming out of the nozzle. The avoidance of droplets is very important because the heaters, made of Mo, can oxidize very easily when in contact with water at high temperatures. A video showing one of the tests is available at [24]. Figure 9 shows some snapshots at different moments of a test.

A steady state is achieved when the complete boiling is occurring at an arbitrary section of the chamber. At this operating state, the power and mass flow rate are adjusted to achieve a constant pressure in the chamber of approximately 5 bar.

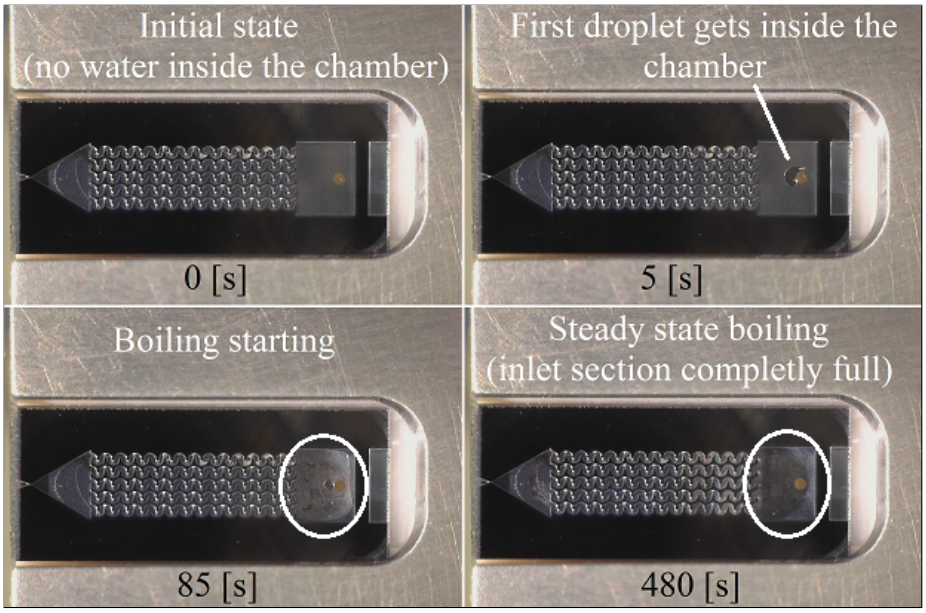

Figure 9: The water is pumped very slowly in the beginning in order to avoid instabilities. Top left corner: water has not yet come inside the chamber; top right corner: water just getting in the chamber; bottom left corner: chamber partially full and boiling; bottom right corner: complete boiling during steady state.

6. Results and discussion

6.1. Mechanical characterization

The structural dimensions have been assessed as described in section 5 with an optical microscope. In table 4 the average measured values are shown and the designed values are in brackets. In general, the averages are slightly smaller than what they were designed.

The depth of the cavities has been measured with a Dektak Surface Profiler and on average they are 100 µm. With these measurements we can recalculate the performance parameters estimated in section 3. As we see in table 5, the mass flow and the thrust are reduced almost by half due to the reduction in the throat width while the specific impulse remains the same. As a consequence the power needed also decreases. Although the differences seen are acceptable, this

Table 4: Average measured values of the dimensions of the thrusters in µm. Design values are in brackets.

type	w_{nd}	l_{nd}	w_{nc}	l_{nc}	w_t	d_1	d_2
L	489.19 ± 2.69 (500)	626.04 ± 3.54 (645)	2978.96 ± 4.19 (3000)	2549.21 ± 5.56 (2600)	25.13 ± 22.90 (45)		
W	777.69 ± 1.51 (780)	643.56 ± 2.81 (660)	2980.40 ± 2.93 (3000)	1489.46 ± 4.88 (1500)	25.99 ± 20.92 (45)		
B	492.62 ± 4.52 (500)	486.94 ± 3.16 (500)	2983.34 ± 2.30 (3000)	1581.32 ± 10.23 (1600)	20.13 ± 13.03 (45)		
d						10.25 ± 0.25 (160)	2.75 ± 0.07 (40)
D						547.74 ± 4.86 (580)	144.30 ± 4.67 (160)
s						76.55 ± 0.14 (60)	8.24 ± 0.89 (20)
S						289.71 ± 7.18 (266)	39.92 ± 2.06 (54)

indicates the need for more precision in the manufacturing to reduce differences between the designed and manufactured devices.

Table 5: Comparison between the design parameters (in brackets) and the ones calculated with the measured values.

Nozzle	$\dot{m}\,[\mathrm{mg\,s^{-1}}]$	$F\,[\mathrm{mN}]$	$I_{sp}\,[\mathrm{s}]$	$P\,[\mathrm{W}]$
L	0.41-1.91	0.43-2.16	107.34-115.60	1.04-5.03
	(0.73-3.42)	(0.75-3.79)	(105.22-112.89)	(1.87-9.01)
W	0.42-1.97	0.45-2.27	108.34-117.22	1.08-5.20
	(0.73-3.42)	(0.77-3.86)	(106.98-115.09)	(1.87-9.01)
B	0.33-1.53	0.35-1.75	107.94-116.51	0.84-4.03
	(0.73-3.42)	(0.75-3.79)	(105.22-112.89)	(1.87-9.01)

The heaters were also measured in order to compare with the designed values. On average each line of the heaters is around 11.3 µm.

The characterization of the surface roughness was done with AFM (Atomic Force Microscopy) using a nTEGRA Aura AFM with NSG10 tip (10 nm tip radius) and a 100 um closed-loop sample scanner. The measurement was done in an area of 40 × 40 µm of a sample that has not been completed in terms of manufacturing since an open device is needed for the measurement. As the last step of the manufacturing is the isotropic etching, we can assume that the roughness of all the surfaces (including the nozzle throat) is similar to the measured roughness of the sample.

Table 6 shows the average values for the measurement. Figure 10 shows the image taken with AFM.

6.2. Electrical characterization

In figure 11 the measurements recorded with the camera are plotted against the resistance measured for four devices. These measurements (done with 10 devices) are used to estimate the value of α as shown in table 7. The average value is $\bar{\alpha} = 1.09 \times 10^{-3}\mathrm{K}^{-1}$ and standard deviation $\sigma_\alpha = 1.79 \times 10^{-4}$ and can be used for other devices that have been manufactured together. An accurate

Table 6: Surface roughness statistical values.

Property	Value
Minimum	$-338.671\,\mathrm{nm}$
Maximum	$391.408\,\mathrm{nm}$
Average value	$11.412\,\mathrm{nm}$
Median	$12.999\,\mathrm{nm}$
R_a (S_a)	$65.223\,\mathrm{nm}$
R_{RMS} (S_q)	$81.803\,\mathrm{nm}$
R_{RMS} (grain-wise)	$81.803\,\mathrm{nm}$
Skew	-0.152
Kurtosis	0.1514
Surface area	$1.678\,34 \times 10^{-9}\,\mathrm{m}^2$
Projected area	$1.601\,57 \times 10^{-9}\,\mathrm{m}^2$
Variation	$438.125\,\mathrm{\mu m}^2$
Entropy	-14.903
Entropy deficit	0.0029304
Inclination θ	$0.03\,\mathrm{deg}$
Inclination ϕ	$165.26\,\mathrm{deg}$

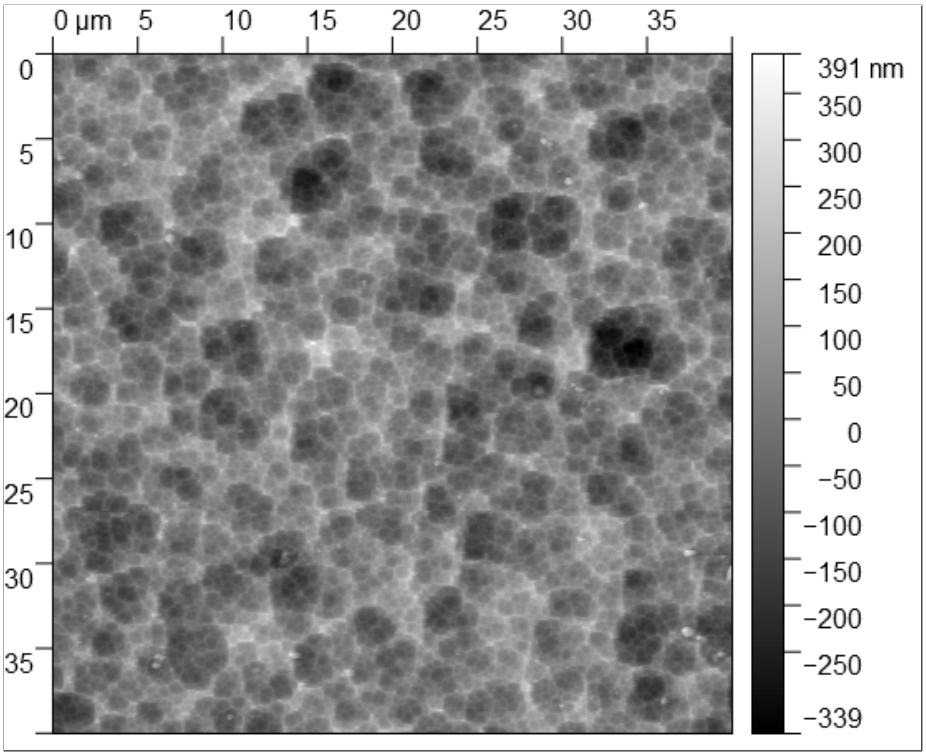

Figure 10: Surface roughness of a sample.

measurement of the initial resistance at room temperature is very important to avoid discrepancies in the estimation of temperature. Figure 12 shows the comparison between the measurements with the thermal camera and the estimation based on (8). The noise seen in the plots comes from the experimental setup that was built using standard equipment with limited precision. This is useful in order mimic the conditions in which the thruster will eventually operate, i.e. in a very small satellite with limited electronics in a harsh environment (i.e. space). As we can see, without considering the noise, the estimation matches very well with the measurements.

6.3. Operational characterization

As mentioned earlier, four thrusters have been tested with water under near-operational conditions but with ambient pressure equal to atmospheric pressure.

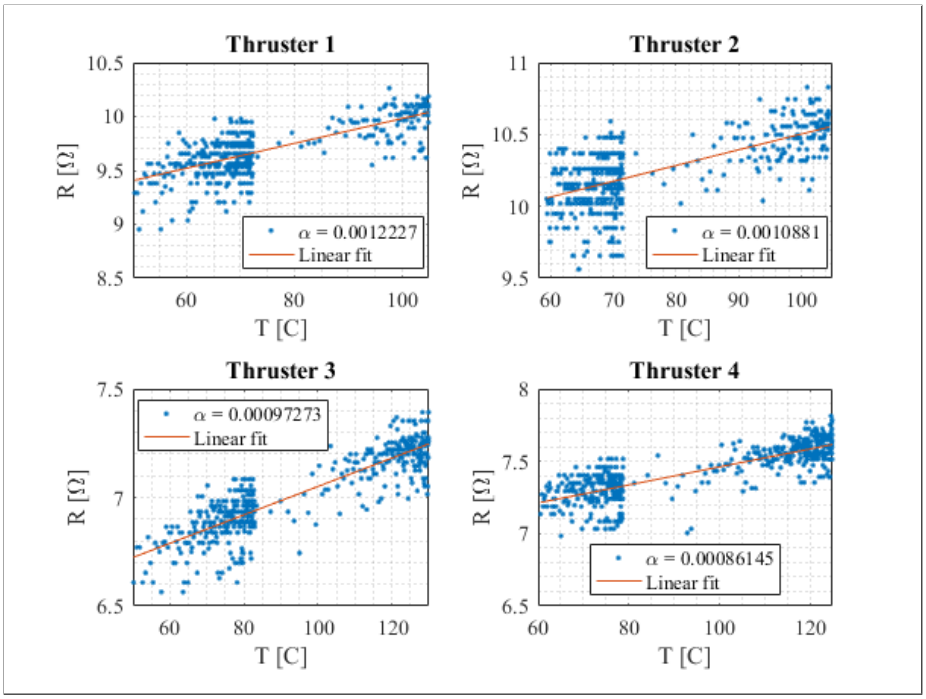

Figure 11: Resistance of the heaters as a function of the temperature for 4 devices.

This high ambient pressure degrades the thrust efficiency but the purpose is to demonstrate the operation of the thrusters.

Water is pumped inside the thruster (very slowly in the beginning) and, after it reaches the inlet section, the power is increased to start the vaporization. When this happens the pressure increases and the power is manually controlled to allow full vaporization (visually) of the propellant. Then, the mass flow rate and the power are kept constant in order to maintain the pressure in the chamber at approximately 5 bar (as mentioned before the control is done manually and with visual feedback). In figure 13 the values of pressure, power, and mass flow rate during the steady state part of the experiment are plotted. We can see that the mass flow rate is not the same even though the nozzle throat area is not much different. The measured values for the throat width are 23.1, 16.5, 20.9 and 23.6 µm for thrusters 5, 7, 9 and 10 respectively. This fact might be attributed to the efficiency in the vaporization which is dependent on the

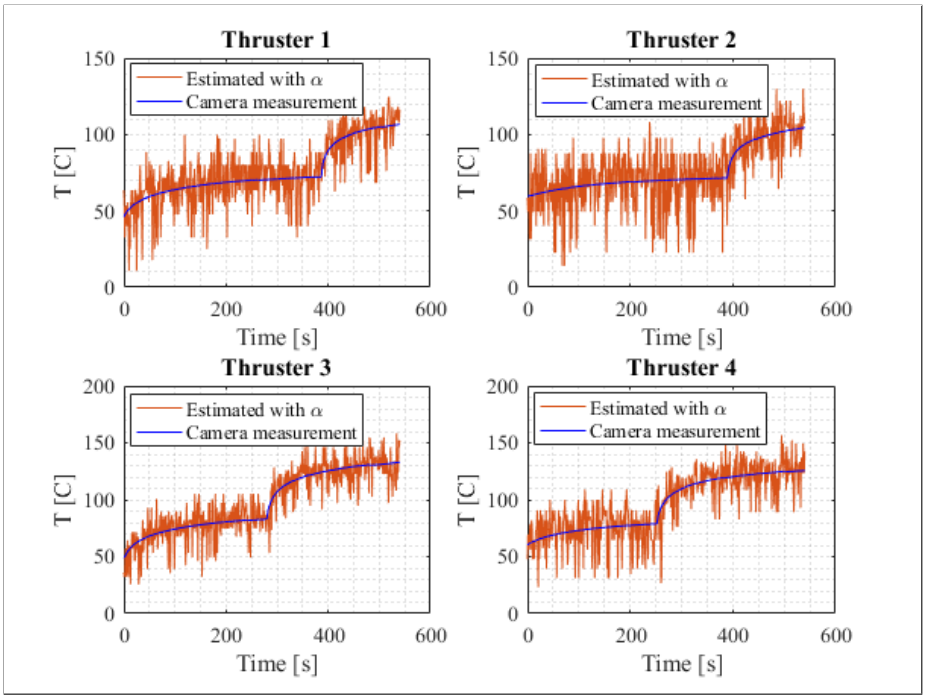

Figure 12: Comparison between estimated and measured values of the temperature of four thrusters.

shape of the microchannels. In table 8 we can see the difference in energy per milli-gram of water used in the process. It is clearly seen that the one with the small diamonds (thruster 9) is the most efficient due to its larger surface area. We can also see in figure 13 the variation in the pressure that is caused by the syringe pump as described in section 5. Although this effect is clearly visible no instability (i.e. no droplets coming out of the nozzle) was spotted during the steady state.

Considering the applied mass flow rate, we can recalculate the power needed to heat-up and vaporize the water and subtract it from the measured power in order to estimate the losses to the structure and the environment which on average for all the tests is around $P_{loss} = 6.17$W. This represents an efficiency in the energy use of around 23% on average.

Figure 14 shows the resistances measured during the steady state and the

Table 7: Values of α for all the thrusters tested.

Thruster	Code	$\alpha\left[\mathrm{K}^{-1}\right]$
1	00-LD1-01	1.30×10^{-3}
2	00-Ld1-01	1.33×10^{-3}
3	00-WD2-01	1.28×10^{-3}
4	00-Bd2-01	8.76×10^{-4}
5	01-LS1-01	1.22×10^{-3}
6	01-BD1-01	1.09×10^{-3}
7	01-BS2-01	9.73×10^{-4}
8	01-WS2-01	8.61×10^{-4}
9	01-Ld1-01	9.55×10^{-4}
10	01-WD2-01	1.01×10^{-3}
Average		1.09×10^{-3}
Standard deviation		1.79×10^{-4}

Table 8: Average values measured during steady state.

Thruster	$p\,[\mathrm{bar}]$	$\dot{m}\left[\mathrm{mg\,s}^{-1}\right]$	$P_{meas}\,[\mathrm{W}]$	$P_{calc}\,[\mathrm{W}]$	$E\left[\mathrm{J\,mg}^{-1}\right]$	Efficiency %
5	4.80	0.55	7.29	1.47	13.16	20
7	5.15	0.75	8.76	1.99	11.71	23
9	5.15	0.83	8.19	2.21	9.84	27
10	5.00	0.61	7.72	1.62	12.66	21

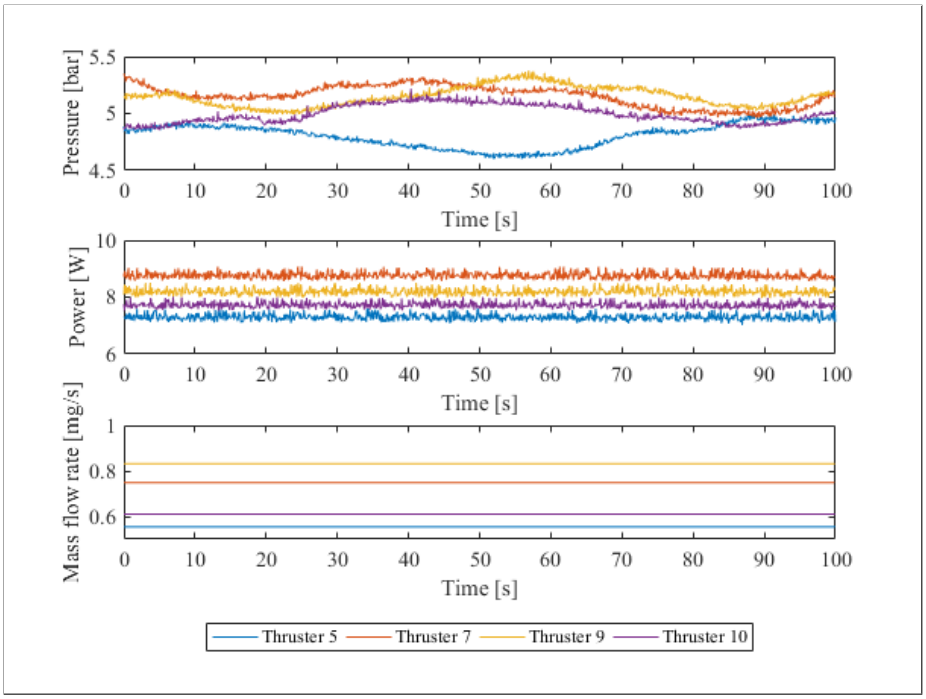

Figure 13: Measured pressure, power, and mass flow rate for the tested devices.

temperature estimated with these values. Given the pressure of water around 5 bar, the saturation temperature is around 151.83 °C. As the power is controlled such that full vaporization occurs, we can consider that this is the temperature that should be measured. This approach is valid for characterization, however in the real operations of the thrusters the power can be set higher to further increase the temperature of the vapor. We can see that the estimated temperature is slightly different for each thruster which can be attributed to differences in the measurements of the initial resistances and initial temperature.

Table 9 presents a comparison of the expected performance in terms of thrust and specific impulse of the devices tested with water and the results of other references found in the literature. The level of thrust is in a range comparable to other devices but it needs to be experimentally measured. The power is the power needed to heat up not only the thruster and the propellant but also the complete interface which has not yet been optimized in terms of thermal

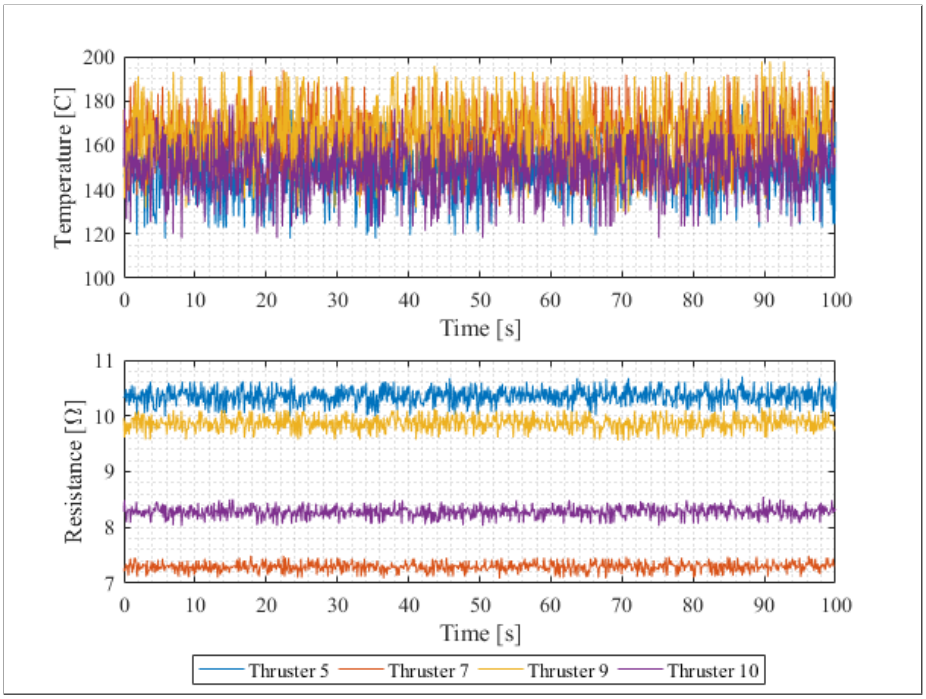

Figure 14: Estimated temperature derived from the measured resistance for the tested devices.

isolation. Also, the tests were conducted in room conditions which means that a significant amount of power is lost to the environment. Therefore, the power consumption of an optimized system in vacuum is expected to be significantly lower than these values.

7. Conclusions

This paper presented the details of the design, manufacturing, and characterization of microresistojets with integrated heating and temperature measurement capabilities that operate by vaporizing water and accelerating the vapor with a convergent-divergent nozzle. In total, 12 devices have been assessed for their mechanical characteristics while 10 of those have undergone an electrical characterization to allow the estimation of temperature using measurements of resistance. Finally, four devices have been tested in near-operational conditions

Table 9: Comparison between the results of this work and other references. The values marked with * are calculated or simulated.

Reference	P [W]	$\dot{m}$ [mg/s]	F [mN]	I_{sp} [s]	p [bar]	T [K]
[25]	n/a	2.33–8.33	2–6.5	65–105	1.0–2.6	454–574
[5]	4.01	1.0	0.634	31	n/a	n/a
[26]	n/a	2.08–16.6 *	1–6 *	48.9–36.9 *	1.0–2.0	423–573
[6]	7.1–9.2	1.0	0.034–0.07	3.42–6.9	1.0	400–422
[7]	1.6–3.6	0.2–2.04	0.15–1.01	50–105	1.0	374–474
[9]	1–2.4	0.7	0.005–0.12	17.5 *	n/a	n/a
[27]	10.8	8.8	0.46	5.33 *	n/a	n/a
[10]	30	0.038	0.003	7.78 *	n/a	n/a
This work						
Thruster 5	7.29	0.55	0.67 *	124.02 *	4.80	423.03
Thruster 7	8.76	0.75	0.88 *	119.80 *	5.15	425.65
Thruster 9	8.19	0.83	0.98 *	120.20 *	5.15	425.65
Thruster 10	7.72	0.61	0.74 *	123.72 *	5.00	424.54

in order to validate the current thruster design and have a glimpse into the operational characteristics of such devices. We successfully demonstrate the operations of the devices using water as propellant and having online measurements of temperature that can be used for feedback control, for example. The results presented here serve to determine the fundamental operational and design characteristics of this kind of propulsion system and will be useful in future implementations.

The manufacturing process has been effective in the sense that most of the devices could be tested with water with the exception of two that have been found blocked. The use of a glass wafer to cover the cavities was very important since it provides a good visualization of the vaporization process and allows the visual control of the operation which would be much more difficult without it. Also, it provides valuable information for automatic control of temperature of the semi stochastic boiling process. However, this will not be necessary in the flight models where no flow visualization is required and a pure silicon wafer can be used.

The use of molybdenum heaters has proved to be a very effective design choice since it is very stable at the temperatures used and can also achieve very high temperatures up to 850 °C. However, the heaters need a protection, such as PECVD silicon oxide, to avoid oxidation at temperatures higher than 350 °C.

The developed interface for testing the thrusters has proved to be very robust and easy to use. The thrusters can be tested right after dicing and they can be reconnected to the interface in a couple of minutes reducing testing time. It provides a good way of connecting the heaters to a power supply without the need of wire bonding and also a leak-free connection for the fluid inlet. The sensor included in the interface provides a measurement of pressure very close to the chamber such that it is safe to assume that the measured values are representative of the ones inside the chamber. This interface also facilitates the fast replacement of thrusters without damaging the devices.

Future research will be focused on the optimization of the channels in the heating chamber in order to improve the heat transfer and the power consump-

tion. A control loop will also be designed to improve the operational performance and focused on the development of a propulsion system that can be used in nano- and pico-satellites. To this purpose, the integration of electronics for the power control of the heaters is currently under investigation. This will represent a large step towards a fully integrated device. The interface for the thrusters will also be improved focused on the reduction of size and thermal isolation. The manufacturing process will be improved by reducing the number of steps, specially in the etching of the cavities cavities, and by including a protection in the heaters to reduce problems with oxidation in high temperatures. The measurements of initial resistance and temperature can be improved in favor of the electrical characterization as well as the measurement of resistance during operation to reduce noise in the estimated temperature. The calibration process will be improved by testing the heaters in a hot plate in vacuum. This is expected to increase the precision of the measurements since a more homogeneous distribution of temperature can be achieved. To this purpose, a new interface has to be developed to facilitate these measurements. More tests will be carried out in vacuum to reduce the heat losses and also using a thrust measurement bench to measure the actual thrust and specific impulse of the devices. Finally, the manufacturing process as well as the mask design will be improved to facilitate the fabrication by reducing process steps and also to reduce differences between the designed and the manufactured devices.

Acknowledgments

The present work was supported by CNPq, Conselho Nacional de Desenvolvimento Científico e Tecnológico Brasil.

References

[1] J. Bouwmeester, J. Guo, Survey of worldwide pico- and nanosatellite missions, distributions and subsystem technology, Acta Astronautica 67 (78) (2010) 854 – 862. doi:http://dx.doi.org/10.1016/j.actaastro.2010.

06.004.
URL http://www.sciencedirect.com/science/article/pii/S0094576510001955

[2] D. Selva, D. Krejci, A survey and assessment of the capabilities of cubesats for earth observation, Acta Astronautica 74 (2012) 50 – 68. doi:http://dx.doi.org/10.1016/j.actaastro.2011.12.014.
URL http://www.sciencedirect.com/science/article/pii/S0094576511003742

[3] C. Boshuizen, J. Mason, P. Klupar, S. Spanhake, Results from the planet labs flock constellation, in: 28th Annual AIAA/USU Conference on Small Satellites, 2014.

[4] K. Lemmer, Propulsion for cubesats, Acta Astronautica In Press, Accepted Manuscript (2017) –. doi:10.1016/j.actaastro.2017.01.048.

[5] K. H. Cheah, K.-S. Low, Fabrication and performance evaluation of a high temperature co-fired ceramic vaporizing liquid microthruster, Journal of Micromechanics and Microengineering 25 (1) (2015) 015013. doi:10.1088/0960-1317/25/1/015013.

[6] K. Karthikeyan, S. Chou, L. Khoong, Y. Tan, C. Lu, W. Yang, Low temperature co-fired ceramic vaporizing liquid microthruster for microspacecraft applications, Applied Energy 97 (0) (2012) 577 – 583, energy Solutions for a Sustainable World - Proceedings of the Third International Conference on Applied Energy, May 16-18, 2011 - Perugia, Italy. doi:10.1016/j.apenergy.2011.11.078.

[7] P. Kundu, T. K. Bhattacharyya, S. Das, Design, fabrication and performance evaluation of a vaporizing liquid microthruster, Journal of Micromechanics and Microengineering 22 (2) (2012) 025016. doi:10.1088/0960-1317/22/2/025016.

[8] D. Maurya, S. Das, S. Lahiri, An analytical model of a silicon {MEMS} vaporizing liquid microthruster and some experimental studies, Sensors and Actuators A: Physical 122 (1) (2005) 159 – 166, {SSSAMW} 04 Special Section of the Micromechanics Section of Sensors and Actuators based on contributions revised from the Technical Digest of the 2004 Solid-State Sensor, Actuator and Microsystems Workshop. doi:10.1016/j.sna.2005.04.020.

[9] D. K. Maurya, S. Das, S. K. Lahiri, Silicon mems vaporizing liquid microthruster with internal microheater, Journal of Micromechanics and Microengineering 15 (5) (2005) 966. doi:10.1088/0960-1317/15/5/010.

[10] X. Ye, F. Tang, H. Ding, Z. Zhou, Study of a vaporizing water microthruster, Sensors and Actuators A: Physical 89 (12) (2001) 159 – 165, special Issue: Micromechanics Section of Sensors and Actuators, based on contributions revised from the Technical Digest of the Thirteenth {IEEE} International Workshop on Micro Electro Mechanical Systems (MEMS-2000). doi:10.1016/S0924-4247(00)00540-9.

[11] M. Mihailovic, T. Mathew, J. Creemer, B. Zandbergen, P. Sarro, Mems silicon-based resistojet micro-thruster for attitude control of nano-satellites, in: Solid-State Sensors, Actuators and Microsystems Conference (TRANSDUCERS), 2011 16th International, 2011, pp. 262–265. doi:10.1109/TRANSDUCERS.2011.5969432.

[12] A. Cervone, V. Pallichadath, M. A. C. Silva, D. Guerrieri, S. Silvestrini, S. Mestry, D. Maxence, B. Zandbergen, H. V. Zeijl, Mems water micro-resistojets for cubesats and pocketqubes, in: MPCS 2017 - International Workshop on Micropropulsion and CubeSats, 2017.

[13] C. A. G. E. Guerrieri DC, Silva MC, Selection and characterization of green propellants for micro-resistojets, ASME Journal of Heat Transfer 139 (10) (2017) 9. doi:10.1115/1.4036619.

[14] L. Mele, F. Santagata, E. Iervolino, M. Mihailovic, T. Rossi, A. Tran, H. Schellevis, J. Creemer, P. Sarro, A molybdenum {MEMS} microhotplate for high-temperature operation, Sensors and Actuators A: Physical 188 (2012) 173 – 180, selected papers from The 16th International Conference on Solid-State Sensors, Actuators and Microsystems. doi:10.1016/j.sna.2011.11.023.

[15] R. Poyck, I. Krusharev, Q. Bellini, B. Zandbergen, A. Cervone, A water-fed micro-resistojet for the delffi formation flying mission, in: International Astronautical Congress, 2014.
URL http://iafastro.directory/iac/paper/id/25415/summary/

[16] G. P. Sutton, O. Biblarz, Rocket propulsion elements, 8th Edition, John Wiley & Sons, 2010.

[17] A. Cervone, B. Zandbergen, D. C. Guerrieri, M. Athayde Costa e Silva, I. Krusharev, H. van Zeijl, Green micro-resistojet research at delft university of technology: new options for cubesat propulsion, CEAS Space Journal Online first (2016) 1–15. doi:10.1007/s12567-016-0135-3.

[18] Te connectivity corporation, accessed in: 12/04/2017 (2017).
URL http://www.te.com/usa-en/product-CAT-BLPS0017.html

[19] F. La Torre, S. Kenjeres, C. R. Kleijn, J.-L. P. Moerel, Effects of wavy surface roughness on the performance of micronozzles, Journal of Propulsion and Power 26 (4) (2010) 655–662. doi:10.2514/1.44828.

[20] Y. Cai, Z. Liu, Z. Shi, Effects of dimensional size and surface roughness on service performance for a micro laval nozzle, Journal of Micromechanics and Microengineering 27 (5) (2017) 055001. doi:10.1088/1361-6439/aa6552.

[21] W. Zeng, I. Jacobi, D. J. Beck, S. Li, H. A. Stone, Characterization of syringe-pump-driven induced pressure fluctuations in elastic microchannels, Lab Chip 15 (2015) 1110–1115. doi:10.1039/C4LC01347F.

[22] W. Zeng, I. Jacobi, S. Li, H. A. Stone, Variation in polydispersity in pump- and pressure-driven micro-droplet generators, Journal of Micromechanics and Microengineering 25 (11) (2015) 115015. doi:10.1088/0960-1317/25/11/115015.

[23] P. M. Korczyk, O. Cybulski, S. Makulska, P. Garstecki, Effects of unsteadiness of the rates of flow on the dynamics of formation of droplets in microfluidic systems, Lab Chip 11 (2011) 173–175. doi:10.1039/C0LC00088D.

[24] M. A. C. Silva, Vaporizing liquid microthruster, accessed in: 01-03-2017 (2017).
URL https://youtu.be/LawZseC6ffQ

[25] J. Cen, J. Xu, Performance evaluation and flow visualization of a {MEMS} based vaporizing liquid micro-thruster, Acta Astronautica 67 (34) (2010) 468 – 482. doi:10.1016/j.actaastro.2010.04.009.

[26] C.-C. Chen, C.-W. Liu, H.-C. Kan, L.-H. Hu, G.-S. Chang, M.-C. Cheng, B.-T. Dai, Simulation and experiment research on vaporizing liquid microthruster, Sensors and Actuators A: Physical 157 (1) (2010) 140 – 149. doi:10.1016/j.sna.2009.10.025.

[27] E. Mukerjee, A. Wallace, K. Yan, D. Howard, R. Smith, S. Collins, Vaporizing liquid microthruster, Sensors and Actuators A: Physical 83 (13) (2000) 231 – 236. doi:10.1016/S0924-4247(99)00389-1.